Journal of Alloys and Compounds 509 (2011) 10080–10085

Contents lists available at ScienceDirect

Journal of Alloys and Compounds

journal homepage: www.elsevier.com/locate/jallcom

Synthesis of vanadium oxide, V_6O_{13} hollow-flowers materials and their application in electrochemical supercapacitors

Zhiyong Huang [a], Hongmei Zeng [a,*], Li Xue [a], Xiangge Zhou [a], Yan Zhao [a,b], Qiongyu Lai [a]

[a] College of Chemistry, Sichuan University, Chengdu 610064, PR China
[b] College of Chemistry and Materials Science, Sichuan Normal University, Chengdu 610068, PR China

ARTICLE INFO

Article history:
Received 31 December 2010
Received in revised form 8 August 2011
Accepted 9 August 2011
Available online 16 August 2011

Keywords:
Vanadium oxide
Hollow-flowers
Mechanism
Supercapacitors

ABSTRACT

Hollow flowers-like V_6O_{13} with an average size of 3 μm was successfully synthesized via a facile sol-hydrothermal approach in a short time. The surface composition, crystalline components and morphology of V_6O_{13} were characterized by X-ray photoelectron spectra (XPS), powder X-ray diffraction (XRD) and scanning electron microscopy (SEM) measurements, respectively. An intercalating-exfoliating-self-assembly model was proposed to explain the formation process of hollow-flower structure based on experimental results. The obtained hollow flowers-like V_6O_{13} exhibits high specific capacitance, good cyclability and low resistance as revealed by analysis of cyclic voltammetry (CV), galvanostatic charge/discharge and electrochemical impedance spectroscopy (EIS). Experimental results also indicate that hollow flowers-like V_6O_{13} can deliver a capacitance of 417 F g^{-1} at a scan rate of 5 mV s^{-1}. This value would decrease to 400 F g^{-1} after 1000 cycles in potential range from 0 to 0.8 V versus saturated calomel electrode (SCE) in 1 mol L^{-1} $NaNO_3$ aqueous electrolyte at pH of 2.

1. Introduction

Supercapacitors are increasingly investigated as potential energy storage solutions due to their higher energy density than conventional capacitors and a higher power density than batteries [1,2]. Generally, supercapacitors are operated based on the electrochemical double-layer capacitance (EDLC) which formed on an electrode/electrolyte interface and a pseudocapacitance which resulted from a fast reversible faradic process of redox-active materials (e.g., metal oxides or conductive polymers). Compared with EDLCs, pseudo-capacitors based on transition metal oxides have much higher energy density [3,4]. Among the numerous materials, various forms of ruthenium oxides [5,6] are clearly noteworthy for their superior electrochemical response. Unfortunately, the expensive nature of ruthenium has limited its technological viability. Subsequently, alternative inexpensive transition metal oxides electrode materials (such as NiO [7,8], MnO_2 [9,10], Co_3O_4 [11]) with good capacitive characteristics have been explored as promising candidates for supercapacitor electrodes.

Over the past decades, vanadium oxides and their derivatives have attracted much attention for their important applications in various fields such as lithium batteries [12–15], actuators [16], sensors [17], catalysis [18], optical switching devices [19], and electrochemical supercapacitors [20–22]. It is worth noting that vanadium oxides (e.g., V_2O_5 [23,24], VO_2(B) [25–27], V_6O_{13} [28,29] are recognized as promising electrode materials for high specific capacitance and accessible layered crystal structures for ion intercalation. However, the operating properties of a battery depend not only on the structure, but also on the morphology of the electrode components [30]. Hence, much effort has been devoted to the synthesis of new electrode materials with one-dimensional (1-D) and 2-D nanostructures such as nanorods [31,32], nanowires [33,34], nanotubes [35,36], nanofibres [37,38], nanobelts [39,40], network [41] in order to improve their electrochemical performances.

Recently, 3-D superstructures containing hollow particles and hollow spheres have attracted considerable attention. Their highly accessible surface area could induce high capacitance and excellent cycling performance in electrochemistry [42]. So far, several vanadium-based hollow spheres have been fabricated by Laser Ablation method [43], template-free hydrothermal approach [44,45], and copolymers [46] and N_2 bubbles [47,48] templating strategies.

Among vanadium oxides, V_6O_{13}, with open structure has a mixture valance of V (V) and V (IV), which has attracted continuous attention as potential cathode material for Li-ion batteries (LIB) since its electrochemical properties were reported by Murphy et al. in 1979 [49]. This is primarily due to their high theoretical energy densities and excellent rechargeability [50–53]. To the best of our knowledge, the current studies of V_6O_{13} have been focusing on 0-D particles [54], 1-D belt-like [55] and 2-D films [56],

* Corresponding author. Tel.: +86 28 85412284.
E-mail address: zenghongmei@scu.edu.cn (H. Zeng).

0925-8388/$ – see front matter © 2011 Elsevier B.V. All rights reserved.
doi:10.1016/j.jallcom.2011.08.042

which were fabricated by thermal decomposition, hydrothermal and plasma enhanced chemical vapor deposition (PECVD) or thermal evaporation, respectively. In our previous work, V_6O_{13} with sheet morphology was applied to be a supercapacitor with high energy density. It was prepared by a thermal decomposing and quenching method with NH_4VO_3 as the starting material [57]. As part of our ongoing research on electrode material of supercapacitors, we herein report the preparation of V_6O_{13} hollow-flowers structure by using O_2 bubbles from the decomposition of H_2O_2 as template through the self-assembly process. Besides, the possible application of V_6O_{13} hollow-flowers as a supercapacitor was also studied in the present work. Based on the experimental results, an intercalating-exfoliating-self-assembly model was proposed to explain the formation mechanism of V_6O_{13} hollow structure. The electrochemical analysis by cyclic voltammetry (CV), galvanostatic charge/discharge and electrochemical impedance spectroscopy indicate that the as-prepared V_6O_{13} could be used as an alternative electrode material for supercapacitors with good electrochemical performance.

2. Experimental

2.1. Materials

All chemicals were used as received without further purification. Bulk vanadium pentaoxide powder (V_2O_5, 99.6%), octylamine ($C_8H_{17}NH_2$, 97%), hydrogen peroxide (H_2O_2, 30%) and all solvents (acetone and absolute ethanol) were of analytical grade.

2.2. Preparation

The V_6O_{13} hollow-flowers were prepared by a facile sol-hydrothermal approach and the detailed process was as followed. Firstly, 0.5 g (2.75 mmol) of commercial bulk V_2O_5 powders were slowly dissolved in a solution of hydrogen peroxide (H_2O_2, 25 mL, 30%) and vigorously stirred at 0 °C by ice-water bathing. An orange solution is formed about 20 min later. Secondly, *n*-octylamine in acetone (1.6 mL, 0.39 g mL^{-1}) was added dropwise to the solution when its' color changed from orange to red after 10 min. Subsequently, the color rechanged into light orange when *n*-octylamines was gradually dissolved and finally turned into brown after 4–6 h. Thirdly, a solution of hydrogen peroxide (1 mL, 30%) was added to the previous solution, leading to a red solution again. The resulting mixture was stirred for 30 min and then transferred into a Teflon-lined autoclave with a stainless-steel shell (50 mL), maintained at 160 °C for 2 days. The resulting black powders were washed with ethanol and deionized water and then dried in air at 80 °C for 12 h. Finally V_6O_{13} hollow-flowers were obtained.

2.3. Characterization

Scanning electron microscopy (SEM, JSM-5900LV, Japan) was employed to observe the structure and morphology of the samples. X-ray powder diffraction (XRD) pattern was collected using a Rigaku D/MAX-rA diffractometer with Cu Kα radiation (λ = 1.5418 Å). XPS analyses were performed using X-ray photoelectron spectroscopy (XPS, XSAM800, Kratos, U.K.) instrument with monochromatic Al Kα radiation and the V 2p and O 1s signals were measured simultaneously in one energy window. The peaks were fitted by the software of XPS peaks in order to resolve the separate constituents after background subtraction. Charge referencing was done with carbon C 1s binding energy of 284.6 eV.

2.4. Electrochemical performance test

The positive electrode was prepared by mixing active material, acetylene black (AB) and polyvinylidene fluoride (PVDF) binder (in a weight ratio of 80:15:5), using *N*-methyl-2-pyrrolidine (NMP) as solvent. After the mixture was blended sufficiently, the obtained slurry was dried in an infrared light oven for 5 h, and then pressed onto a stainless-steel grid. For most cases, the mass loading of active vanadium oxide material in the electrode was 25 g m^{-2}. The negative electrode was prepared by the same method mentioned above and it consisted of 65 wt% activated carbon (AC), 29 wt% AB and 6 wt% PVDF. The electrolyte for the test was 1 mol L^{-1} $NaNO_3$ with pH of 2. All the charge/discharge tests were performed by using Neware Cell Program Control Test System with current density of 100 and 200 mA g^{-1} in the range of 0–0.8 V at room temperature, which contains a two-electrode system.

Cyclic voltammetry (CV) measurements were performed by using a three-electrode system, in which active materials were used as the working electrode, platinum as the counter electrode, and saturated calomel electrode (SCE) as the reference electrode. The measurement was carried out on a Tianjin Lanlike Electrochemical Workstation (model LK2006) with the electrochemical interface controlled by computer. Electrochemical impedance spectroscopy (EIS) measurements were carried out at frequencies from 10 kHz to 0.01 Hz by using an Autolab Electrochemical Workstation, which consists of a three-electrode system with active material working electrode, platinum counter electrode and SCE reference electrode. The electrochemical interface and frequency response analyzer were controlled by a computer.

3. Results and discussion

3.1. XRD analysis

Fig. 1a shows the XRD pattern of as-synthesized products. Most of the diffraction peaks in Fig. 1a can be indexed to the V_6O_{13} phase (JCPDS 89-0100), as shown in Fig. 1b. However, the broad and low diffraction peaks indicate that the as-synthesized products have weak crystalline structure.

3.2. XPS analysis

The XPS wide-range scan of as-synthesized sample is presented in Fig. 2a. XPS analysis reveals that the as-synthesized materials are composed of V, O, C and N elements. C and N are mainly from the organic starting materials that still remain in the final samples. The binding energies obtained in the XPS analysis were corrected for specimen charging by referencing the C 1s line to 284.6 eV. The XPS spectra of V 2p together with O 1s are presented in Fig. 2b. The fitted peaks at 529.8, 531.1, and 532.2 eV can be assigned to the O^{2-} in V=O, V–O and absorbed H_2O, respectively. The results show that more than one oxygen species exists in the as-prepared sample [58,59]. The peaks of both V $2p_{3/2}$ and V $2p_{1/2}$ were decomposed at 517.5, 516.7 eV and 524.8, 524 eV, corresponding to V(V) (524.8,

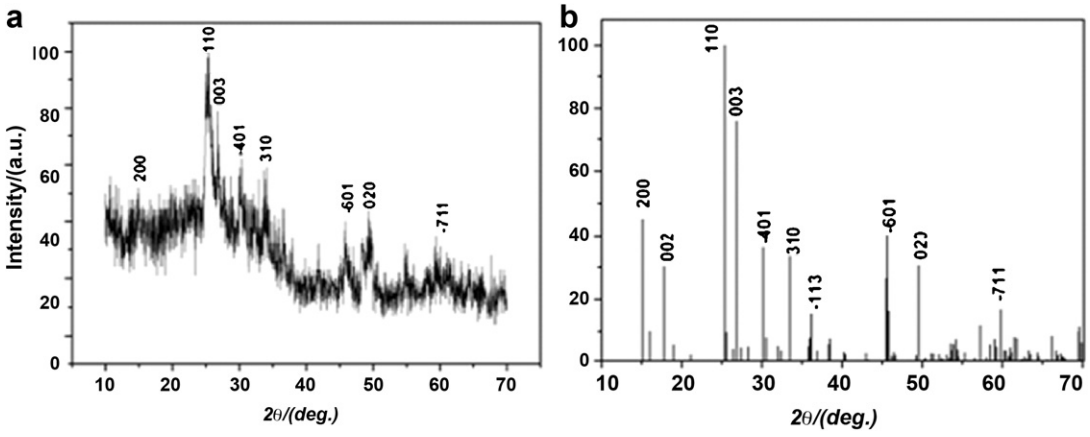

Fig. 1. (a) XRD pattern for the sample V_6O_{13} hollow-flowers. (b) XRD pattern for the pure sample V_6O_{13} (JCPDS card no.89-0100).

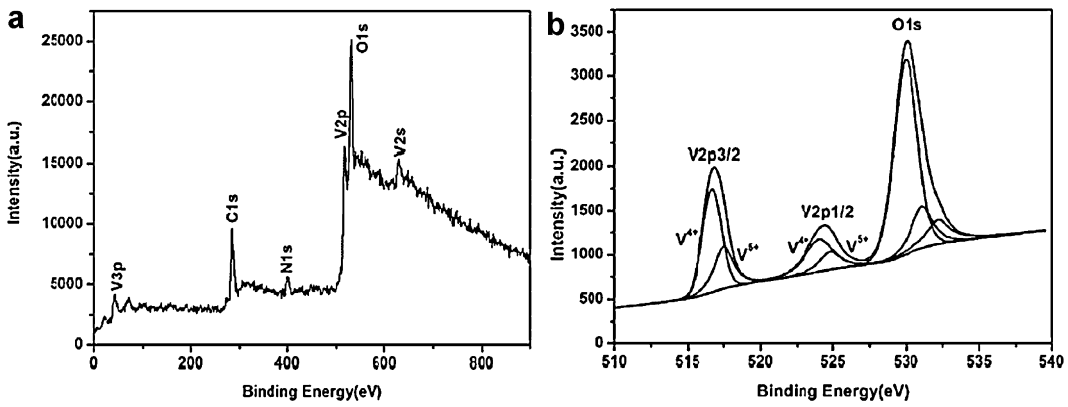

Fig. 2. (a) Survey XPS spectrum of V_6O_{13} hollow-flowers. (b) Fitted curves for HRXPS spectrum of V 2p and O 1s region.

517.5 eV) and V(IV) (524, 516.7 eV), respectively [60]. The calculated ratio of 1:2.1 for V (V):V (IV) deduced from the area under the V $2p_{3/2}$ peak indicates that the sample is V_6O_{13}.

3.3. SEM analysis

Fig. 3 shows the SEM images of the samples prepared at different conditions. As shown in Fig. 3a–e, the samples exhibit hollow flower-like morphology, when 30% H_2O_2 was adopted in the final step of preparation. As shown in the high magnification SEM images (see Fig. 3b–e), the microspheres with an average diameter of 3.0 μm are made up of numerous nanoflake-like petals. The accumulation of nanoflake-like petal made the sphere become hollow structure. However, when H_2O_2 was not added in the final preparation step, only some agminated flakes can be observed (as shown in Fig. 3i and j). Moreover, no dissociative hydrogen peroxide can be detected in the solution 3 h later [61]. These results indicate that the final addition of H_2O_2 may play an important role in the formation of hollow flower-like morphology. The 15% H_2O_2 was subsequently employed instead of 30% H_2O_2 in the final step of preparation and led to less hollow flower-like morphology observed (Fig. 3f–h). Thus, the above hypothesis seems very plausible.

3.4. Possible formation process

Based on the above results of XRD, XPS, and SEM, an intercalating-exfoliating-self-assembly model was proposed to illustrate the formation of hollow flower-like morphology (as shown

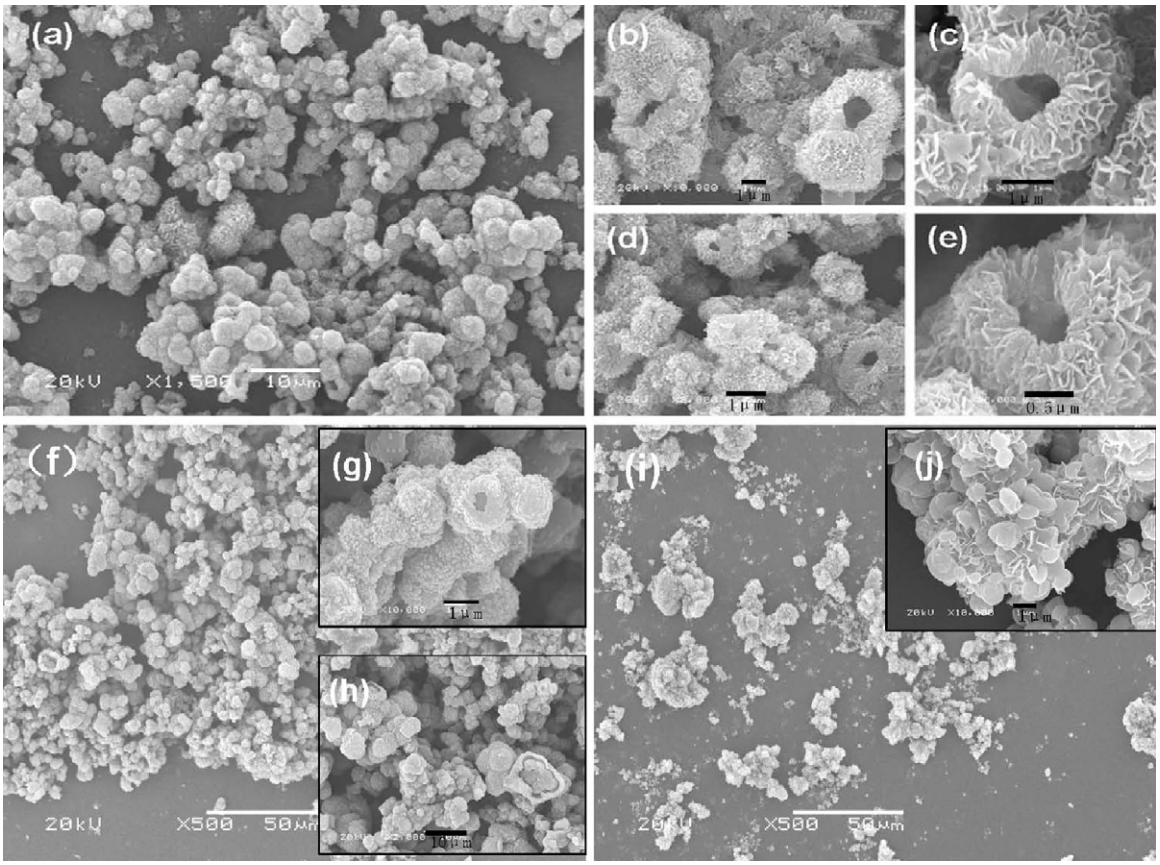

Fig. 3. SEM images of the samples at different reaction condition: (a–e) adding 30% H_2O_2 in the final step of preparation, (f–h) adding 15% H_2O_2 in the final step of preparation, (i–j) without adding H_2O_2 in the final step of preparation.

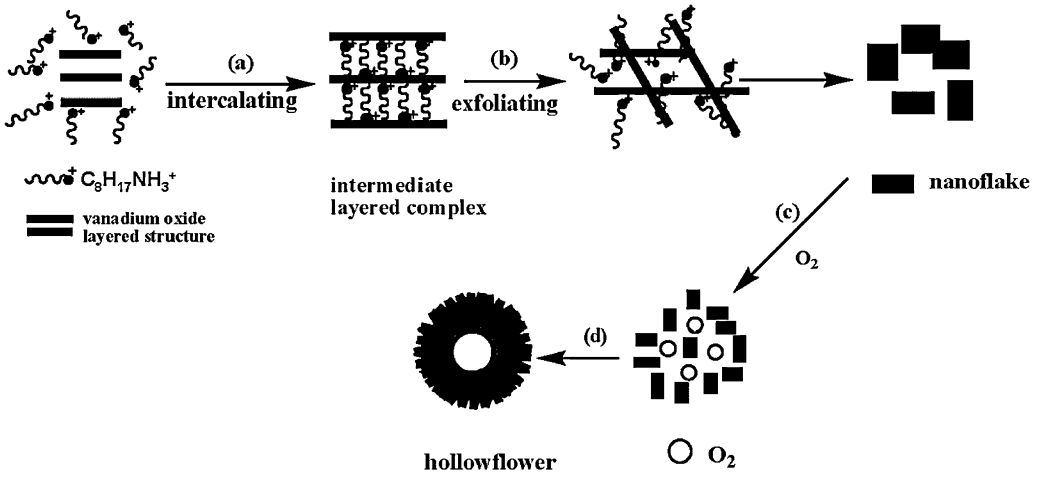

Scheme 1. Illustration of the possible formation process of V_6O_{13} hollow-flowers.

in Scheme 1). It is well known that organic amines intercalate the layers of vanadium oxide to form lamellar structures via the rearrangement of the vanadium oxide structure. The rearrangement is caused by the reduction of some V (V) species to V (IV) species. This reduction is promoted by thermal decomposition of some amines [62]. Finally, lamellar sheets start to roll up to form VO_x nanotubes [63,64]. In this study, protonated *n*-octylamine in the acidic V_2O_5 sols is directly intercalated into vanadium oxide layers to form intermediate complex and then the layers are gradually exfoliated to form nanoflakes (step a and b). Similar models for the formation of layered structures as intermediate have been reported [65,66]. O_2 bubbles, from the decomposition of H_2O_2, can work as the soft templates of self-assembly to drive nanofakes finally to form hollow-flowers by the minimization of the interfacial energy (step c and d). Similar TiO_2 hierarchical hollow spheres were prepared by using the same soft templates of O_2 bubbles [67]. Thereby, H_2O_2 is not only the reagent but also the source of O_2 bubbles in the formation of hollow flowers-like V_6O_{13}. Furthermore, its concentration also has effect on the structure of the sample in the present work.

3.5. Electrochemical analysis

3.5.1. CV analysis

In order to investigate the electrochemical properties, the cyclic voltammetry of obtained active sample was performed. The scanning potential window was from 0 to 0.8 V (VS. SCE), which can eliminate the current tailing derived from the oxygen and hydrogen of evolution. Fig. 4 shows the CV curves of V_6O_{13} in the potential range of 0 to 0.8 V (vs. SCE) at different scan rates of 3–20 mV s^{-1} in 1 mol L^{-1} $NaNO_3$ aqueous electrolyte at pH of 2. All CV curves of the samples exhibit a quasi rectangular shape in the given potential range, and the *I-E* responses are almost symmetric with respect to the zero-current line, showing the characteristic feature of capacitive behavior [68]. However, the shapes of the CV curves become slant gradually with the increase of scan rate, which might be caused by polarization [69]. Furthermore, the voltammograms of Fig. 4 is not ideal because of the pseudo-capacitive behavior of vanadium oxide due to redox-process of intercalation-deintercalation (or adsorption-desorption) of cation species on the surface of the material [70]. Moreover, V (V) to V (IV) shuttle redox reaction could occur for this material, which can explain capacitance values around at 400 F g^{-1}. The single electrode discharge specific capacitance can be estimated from the voltammetric charge surrounded by the CV curve according to the following equation [71]:

$$c = \frac{q_a + |q_c|}{2w\Delta V} \quad (1)$$

where $(q_a + |q_c|)$ is the sum of anodic and cathodic voltammetric charges on positive and negative sweeps, w is the mass of active material and ΔV is the potential window of CV. Based on Eq. (1), the highest single electrode discharge specific capacitance is 417 F g^{-1} at a scan rate of 5 mV s^{-1}. These high performances could be contributed to the large specific surface area of the sample. The special shape of hollow-flowers would promote active material to contact with electrolyte sufficiently and increase the effective availability of active material [45].

3.5.2. Galvanostatic charge/discharge test

Current density is one of the important factors influencing the capacitive behavior of the supercapacitor. Galvanostatic charge/discharge measurements were carried out to get insight into the capacitance characteristic of the samples at different current densities. The measurements were carried out in the potential range from 0 to 0.8 V. Fig. 5 shows the charge/discharge behavior of capacitors at different current densities of 100 and 200 mA g^{-1}, respectively, in 1 mol L^{-1} $NaNO_3$ aqueous electrolyte at pH of 2. A good linear variation of potential vs. time is observed for all charge/discharge curves. The charge curves are symmetric to their corresponding discharge counterparts, and the voltage drop is not

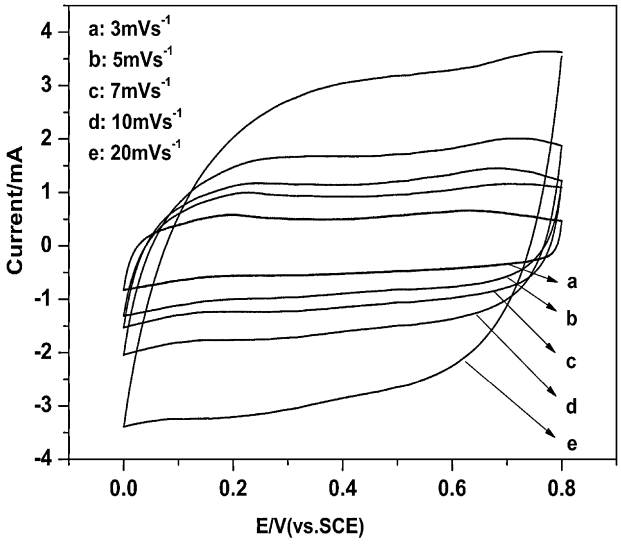

Fig. 4. CV curves of the V_6O_{13} electrode at different scan rates in 1 mol L^{-1} $NaNO_3$ aqueous electrolyte at pH of 2.

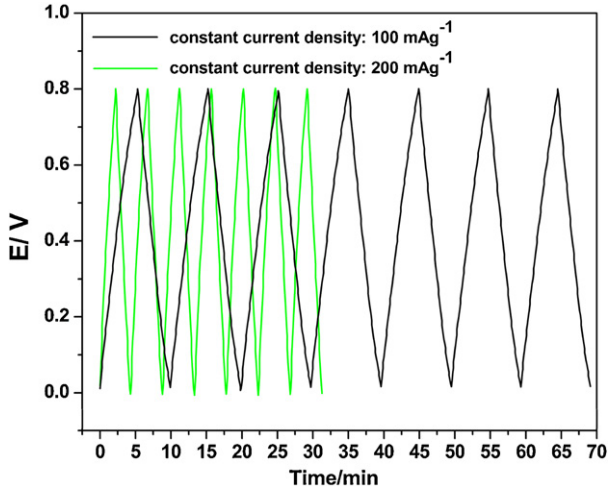

Fig. 5. Charge/discharge curves of the V_6O_{13}/AC asymmetric supercapacitor at different current densities in 1 mol L^{-1} $NaNO_3$ aqueous electrolyte at pH of 2.

observed. The results imply that V_6O_{13} hollow-flower material has a good capacitive behavior. As can be seen from Fig. 5, the specific capacitance obtained at the current density of 100 mA g^{-1} is a little higher than that of at 200 mA g^{-1}. This might be because, at low current density, there is enough time for the cations to intercalate into the samples. As reported in our previous study [57], the charge storage mechanism of V_6O_{13} hollow-flower is mainly a surface process, which involves ion-electrons mechanism.

As the above equation depicted, M^+ ions could easily intercalate into interlayer and electron transfer from the electrolyte to the V_6O_{13} electrode under discharging state. This might be ascribed to its special hollow-flower structure which would provide more sites for the adsorption of M^+. On the other hand, under charging state, M^+ ions also could conveniently extract from host phase and electrons back to the electrolyte.

3.5.3. Cycling stability of hybrid supercapacitor

Fig. 6 shows the cycling ability of the obtained sample at current densities of 100 and 200 mA g^{-1} in 1 mol L^{-1} $NaNO_3$ aqueous electrolyte at pH of 2. The data illustrate that this material exhibited excellent capacity retention, in particular at a current density of 100 mA g^{-1}. The capacitance value only slightly decreased with the increase of cycling times.The initial value of 417 F g^{-1} decreased to 400 F g^{-1} after 1000 cycles. Meanwhile, when current density was

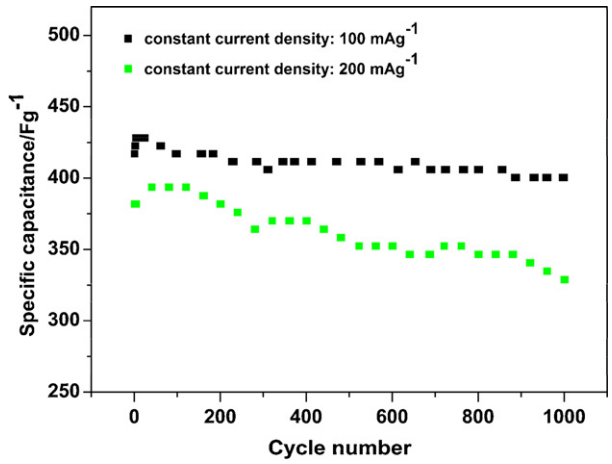

Fig. 6. Cycling ability of V_6O_{13} at different current densities in 1 mol L^{-1} $NaNO_3$ aqueous electrolyte at pH of 2.

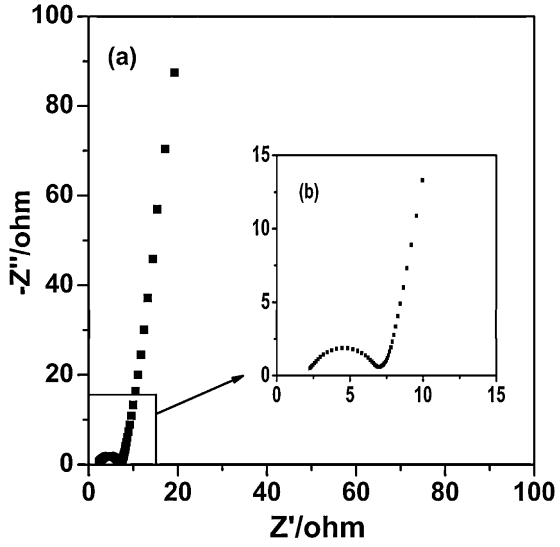

Fig. 7. Electrochemical impedance plots of V_6O_{13} electrode in 1 mol L^{-1} $NaNO_3$ aqueous electrolyte at pH of 2.

increased to 200 mA g^{-1}, the capacitance value remained 329 F g^{-1} after 1000 cycles.

3.5.4. Electrochemical impedance measurement

Impedance spectroscopy technique was applied to investigate the electrochemical behavior of the supercapacitor. As shown in Fig. 7, the obtained curve of impedance showes two typical parts: a high frequency semicircle and a low frequency straight line due to the resistance of electrode-electrolyte interfacial charge transfer and the diffusion-controlled electrode kinetics, respectively [4,72]. As depicted in Fig. 7b, the resistance of charge transfer associated with the surface properties should be small according to its small diameter in high frequency semicircle. The result of small charge transfer resistance might attribute to the larger contact area between electrode and electrolyte. In addition, the straight line in low-frequency range is inclined at angle of nearly 90°to the real axis, indicating that the capacitor has a good capacitive behavior. The result is consistent with cyclic voltammograms and galvanostatic charge/discharge tests.

4. Conclusions

In summary, hollow flowers-like V_6O_{13} with an average size of 3 μm has been successfully prepared via a facile sol-hydrothermal approach. Furthermore, an intercalating-exfoliating-self- assembly model was proposed to explain the formation process of hollow-flowers structure. The low resistance, high capacitance (417 F g^{-1}) as well as good cyclic stability can be attributable to hollow-flowers structure with a higher surface area, shorter ion diffusion pathways. Thereby, the obtained hollow flowers-like V_6O_{13} could become a promising electrode material for supercapacitors due to its good electrochemical performance.

References

[1] S. Sarangapani, B.V. Tilak, C.P. Chen, J. Electrochem. Soc. 143 (1996) 3791–3799.
[2] Y. Yang, D.H. Kim, M. Yang, P. Schmuki, Chem. Commun. 47 (2011) 7746–7748.
[3] C.C. Hu, T.W. Tsou, Electrochem. Commun. 4 (2002) 105–109.
[4] L.M. Chen, Q.Y. Lai, Y.J. Hao, Y. Zhao, X.Y. Ji, J. Alloys Compd. 467 (2009) 465–471.
[5] J.P. Zheng, Electrochem. Solid-State Lett. 2 (1999) 359–361.
[6] K. Kuratani, T. Kiyobayashi, N. Kuriyama, J. Power Sources 189 (2009) 1284–1291.
[7] J.W. Lee, T.B. Ahn, J.H. Kim, J.M. Ko, J.D. Kim, Electrochim. Acta 56 (2011) 4849–4857.

[8] D.S. Kong, J.M. Wang, H.B. Shao, J.Q. Zhang, C.N. Cao, J. Alloys Compd. 509 (2011) 5611–5616.
[9] J.H. Cheng, G. Shao, H.J. Yu, J.X. Xu, J. Alloys Compd. 505 (2010) 163–167.
[10] L. Yi, H.Q. Xie, J.F. Wang, L.F. Chen, Mater. Lett. 65 (2011) 403–405.
[11] Y.H. Li, K.L. Huang, S.Q. Liu, Z.F. Yao, S.X. Zhuang, J. Solid State Electrochem. 15 (2011) 587–592.
[12] Y.C. Si, L.F. Jiao, H.T. Yuan, H.X. Li, Y.M. Wang, J. Alloys Compd. 486 (2009) 400–405.
[13] S.M. Lee, H.S. Kim, T.Y. Seong, J. Alloys Compd. 509 (2011) 3136–3140.
[14] C. Cai, D.S. Guan, Y. Wang, J. Alloys Compd. 509 (2011) 909–915.
[15] S.Q. Wang, Z.D. Lu, D. Wang, C.G. Li, C.H. Chen, Y.D. Yin, J. Mater. Chem. 21 (2011) 6365–6369.
[16] G. Gu, M. Schmid, P.W. Chiu, M. Kozlov, E. Munoz, R.H. Baughman, Nat. Mater. 2 (2003) 316–319.
[17] E. Strelcov, Y. Lilach, A. Kolmakov, Nano Lett. 9 (2009) 2322–2326.
[18] H. Nair, J.E. Gatt, J.T. Miller, C.D. Baertsch, J. Catal. 279 (2011) 144–154.
[19] C.Z. Wu, H. Wei, B. Ning, Y. Xie, Adv. Mater. 22 (2010) 1972–1976.
[20] H.Y. Lee, J.B. Goodenough, J. Solid State Chem. 148 (1999) 81–84.
[21] J.M. Li, K.H. Chang, C.C. Hu, Electrochem. Commun. 12 (2010) 1800–1803.
[22] L.M. Chen, Q.Y. Lai, H.M. Zeng, Y.J. Hao, J.H. Huang, J. Appl. Electrochem. 41 (2011) 299–305.
[23] Y. Wang, G. Cao, Chem. Mater. 18 (2006) 2787–2804.
[24] Y.Y. Liu, M. Clark, Q.F. Zhang, D.M. Yu, D.W. Liu, J. Liu, G.Z. Cao, Adv. Energy Mater. 1 (2011) 194–202.
[25] C. Tsang, A. Manthiram, J. Electrochem. Soc. 144 (1997) 520–524.
[26] E. Baudrin, G. Sudant, D. Larcher, B. Dunn, J.M. Tarascon, Chem. Mater. 18 (2006) 4369–4374.
[27] S.D. Zhang, Y.M. Li, C.Z. Wu, F. Zheng, Y. Xie, J. Phys. Chem. C 113 (2009) 15058–15067.
[28] C.L. Onnerud, J.O. Thomas, M. Hardgrave, S.Y. Anderson, J. Electrochem. Soc. 142 (1995) 3648–3651.
[29] K. West, B.Z. Christiansen, T. Jacobsen, S. Atlung, J. Power Sources 14 (1985) 235–245.
[30] W.U. Huynh, J.J. Dittmer, A.P. Alivisatos, Science 295 (2002) 2425–2427.
[31] Z. Gui, R. Fan, W.Q. Mo, X.H. Chen, L. Yang, S.Y. Zhang, Y. Hu, Z.Z. Wang, W.C. Fan, Chem. Mater. 14 (2002) 5053–5056.
[32] N. Rama, M.S. Ramachandra Rao, Solid State Commun. 150 (2010) 1041–1044.
[33] Z. Chen, Y.C. Qin, D. Weng, Q.F. Xiao, Y.T. Peng, X.L. Wang, H.X. Li, F. Wei, Y.F. Lu, Adv. Funct. Mater. 19 (2009) 3420–3426.
[34] L.Q. Mai, Y.J. Dong, L. Xu, C.H. Han, Nano Lett. 10 (2010) 4273–4278.
[35] C.J. Cui, G.M. Wu, J. Shen, B. Zhou, Z.H. Zhang, H.Y. Yang, S.F. She, Electrochim. Acta 55 (2010) 2536–2541.
[36] A.I. Popa, E. Vavilova, C. Taschner, V. Kataev, B. Buchner, R. Klingeler, J. Phys. Chem. C 115 (2011) 5265–5270.
[37] E.A. Ponzio, T.M. Benedetti, R.M. Torresi, Electrochim. Acta 52 (2007) 4419–4427.
[38] G. Wee, H.Z. Soh, Y.L. Cheah, S.G. Mhaisalkar, M. Srinivasan, J. Mater. Chem. 20 (2010) 6720–6725.
[39] H. Qiao, X.J. Zhu, Z. Zheng, L. Liu, L.Z. Zhang, Electrochem. Commun. 8 (2006) 21–26.
[40] D.A. Semenenko, D.M. Itkis, E.A. Pomerantseva, E.A. Goodilin, T.L. Kulova, A.M. Skundin, Y.D. Tretyakov, Electrochem. Commun. 12 (2010) 1154–1157.
[41] E. Khoo, J.M. Wang, J. Ma, P.S. Lee, J. Mater. Chem. 20 (2010) 8368–8374.
[42] X.W. Lou, Y. Wang, C.L. Yuan, J.Y. Lee, L.A. Archer, Adv. Mater. 18 (2006) 2325–2329.
[43] R. Levi, M.B. Sadan, A.A. Yaron, R.P. Biro, L. Houben, C. Shahar, A. Enyashin, G. Seifert, Y. Prior, Reshef Tenne, J. Am. Chem. Soc. 132 (2010) 11214–11222.
[44] L.J. Mao, C.Y. Liu, J. Li, J. Mater. Chem. 18 (2008) 1640–1643.
[45] H.M. Liu, Y.G. Wang, K.X. Wang, E.J. Hosono, H.S. Zhou, J. Mater. Chem. 19 (2009) 2835–2840.
[46] A.M. Cao, J.S. Hu, H.P. Liang, L.J. Wan, Angew. Chem. Int. Ed. 44 (2005) 4391–4395.
[47] C. Wu, Y. Xie, L. Lei, S.Q. Hu, C.Z.O. Yang, Adv. Mater. 18 (2006) 1727–1732.
[48] D.M. Rojas, E. Baudrin, Solid State Ionics 178 (2007) 1268–1273.
[49] D.W. Murphy, P.A. Christian, F.J. Disalo, J. Electrochem. Soc. 126 (1979) 497–499.
[50] M.Y. Saïdi, R. Koksbang, E.S. Saïdi, H. Shi, J. Barker, J. Power Sources 68 (1997) 726–729.
[51] T. Schmitt, A. Augustsson, J. Nordgren, L.C. Duda, Appl. Phys. Lett. 86 (2005) 064101.
[52] C. Leger, S. Bach, J.P. Pereira-Ramos, J. Solid State Electrochem. 11 (2007) 71–76.
[53] A. Rúa, F.E. Fernández, R. Cabrera, N. Sepúlveda, J. Appl. Phys. 105 (2009) 113504.
[54] O. K. Chang, M. Y. Saidi, USA U.S. US 5, 545, 496.
[55] X.Y. Xu, X.G. Li, Chin. Chem. Lett. 16 (2005) 249–252.
[56] J.G. Zhang, P. Liu, J.A. Turner, C.E. Tracy, D.K. Benson, J. Electrochem. Soc. 145 (1998) 1889–1892.
[57] H.M. Zeng, Y. Zhao, Y.J. Hao, Q.Y. Lai, J.H. Huang, X.Y. Ji, J. Alloys Compd. 477 (2009) 800–804.
[58] G. Silversmit, D. Depla, H. Poelman, G.B. Marin, R.D. Gryse, J. Electron Spectrosc. Relat. Phenom. 135 (2004) 167–175.
[59] T.D. Nguyen, T.O. Do, Langmuir 25 (2009) 5322–5332.
[60] Y.L. Wang, X.K. Chen, M.C. Li, R. Wang, G. Wu, J.P. Yang, W.H. Han, S.Z. Cao, L.C. Zhao, Surf. Coat. Technol. 201 (2007) 5344–5347.
[61] B. Alonso, J. Livage, J. Solid State Chem. 148 (1999) 16–19.
[62] C. Huang, X.Q. Li, L.B. Kong, H.J. Zhou, Y.Q. Li, J.W. Qiu, Y.Y. Wang, Rare Metals 25 (2006) 88–93.
[63] A. Bouhaouss, P. Aldebert, Mater. Res. Bull. 18 (1983) 1247–1256.
[64] W. Chen, J.F. Peng, L.Q. Mai, Q.Y. Zhu, Q. Xu, Mater. Lett. 58 (2004) 2275–2278.
[65] M.D. Wei, H. Sugihara, I. Honma, M. Ichihara, H.S. Zhou, Adv. Mater. 17 (2005) 2964–2969.
[66] M.D. Wei, Y. Konishi, H.S. Zhou, H. Sugihara, H. Arakawa, Chem. Phys. Lett. 400 (2004) 231–234.
[67] X.X. Li, Y.J. Xiong, Z.Q. Li, Y. Xie, Inorg. Chem. 45 (2006) 3493–3495.
[68] M. Jayalakshmi, M.M. Rao, N. Venugopal, K.B. Kim, J. Power Sources 166 (2007) 578–583.
[69] J. Yan, E. Khoo, A. Sumboja, P.S. Lee, ACS Nano 4 (2010) 4247–4255.
[70] L. Yu, C.X. Zhao, X. Long, W. Chen, Microporous Mesoporous Mater. 126 (2009) 58–64.
[71] Y. Zhao, Q.Y. Lai, Y.J. Hao, H.M. Zeng, H.Y. Chu, Z.E. Lin, J. Power Sources 195 (2010) 4400–4405.
[72] M.S. Dandekar, G. Arabale, K. Vijayamohanan, J. Power Sources 141 (2005) 198–203.